Taylor & Francis
Taylor & Francis Group

Phase Transitions
A Multinational Journal

ISSN: (Print) (Online) Journal homepage: https://www.tandfonline.com/loi/gpht20

Preparation and characterization of $NiFe_2O_4$ thin films for supercapacitor applications

Vidyadevi A. Jundale, Dilip A. Patil & Abhijit A. Yadav

To cite this article: Vidyadevi A. Jundale, Dilip A. Patil & Abhijit A. Yadav (2022) Preparation and characterization of $NiFe_2O_4$ thin films for supercapacitor applications, Phase Transitions, 95:11, 786-802, DOI: 10.1080/01411594.2022.2122825

To link to this article: https://doi.org/10.1080/01411594.2022.2122825

Published online: 20 Sep 2022.

PHASE TRANSITIONS
2022, VOL. 95, NO. 11, 786–802
https://doi.org/10.1080/01411594.2022.2122825

Preparation and characterization of $NiFe_2O_4$ thin films for supercapacitor applications

Vidyadevi A. Jundale[a,b], Dilip A. Patil[c] and Abhijit A. Yadav [a]

[a]Thin Film Physics Laboratory, Department of Physics, Electronics and Photonics, Rajarshi Shahu Mahavidyalaya (Autonomous), Latur, India; [b]Department of Engineering Science and Humanities, SRES's Sanjivani College of Engineering, Kopargaon, India; [c]Mechanical Department, Sanjivani KBP Polytechnic, Kopargaon, India

ABSTRACT

Mesoporous $NiFe_2O_4$ thin films have been prepared by chemical spray pyrolysis. The films are characterized by XRD, FESEM, EDAX, UV-Visible spectroscopy, DC electrical resistivity and electrochemical measurements. XRD result shows the cubic crystal structure with Fd-3 m (227) space group. Crystallite size is found in the range of 14–21 nm. FESEM showed crack free, well defined, uniform, mesoporous spherical grain-like surface morphology. EDAX study confirmed nearly stoichiometric deposition. The optical absorption studies confirmed direct allowed type transition with bandgap in the range of 2.09–2.29 eV. The films showed room temperature electrical resistivity of 2.34×10^4 Ωcm. The $NiFe_2O_4$ thin film spray deposited at 450°C exhibited a specific capacitance of 591 Fg^{-1} at a scan rate of 5 $mV{\cdot}s^{-1}$ from CV and specific capacitance of 632 Fg^{-1} at a current density of 0.5 Ag^{-1} from GCD. These findings recommend a constructive route towards the preparation of $NiFe_2O_4$ electrodes for high-performance electrochemical supercapacitors.

ARTICLE HISTORY
Received 18 May 2022
Accepted 5 September 2022

KEYWORDS
Spray pyrolysis; $NiFe_2O_4$; supercapacitor; electrochemical impedance spectroscopy

1. Introduction

Energy is important for human development and maintaining the quality of life. Energy production, which rest on the combustion of fossil fuels, is affecting the world economy and ecology rigorously [1,2]. There has been an increasing demand for environment friendly, high performance renewable energy storage devices. Electrochemical energy is an inevitable part of the clean energy portfolio [3–5]. Batteries, supercapacitors and fuel cells are exceptional energy storage devices working on the principle of electrochemical energy conversion. Amongst these, supercapacitors are emerging as one of most important and promising energy storage devices because of its number of abilities including high power density, rapid charge–discharge rate, safe for handling and long life [6–11]. Supercapacitors are categorized into electric double-layer capacitor (EDLC) and pseudocapacitor [12]. In EDLC, the charge separation at the active electrode and electrolyte solution is responsible for storage of the electrochemical energy. In EDLC, mostly activated carbon, graphene oxide and carbon materials are used as electrodes. While in pseudocapacitor, electrochemical energy is stored due to faradaic reaction between active electrode (conducting polymer or transition metal oxide) and electrolyte solution [13–16]. The energy storage capacity of transition metal oxides is higher as compared to EDLC materials because of its rapid reversible faradaic reactions [17]. The electrode materials in thin film form have few advantages and disadvantages, which should be considered for their specific practical applications. For example, carbon based thin film electrode shows

CONTACT Abhijit A. Yadav aay_physics@yahoo.co.in

the high conductivity, long cycling stability but low specific capacitance, whereas metal oxide thin films exhibit large specific capacitance but suffer from poor conductivity; conducting polymers have large specific capacitance and good conductivity and poor cycling stability [18].

The transition metal oxides have been explored as a material for supercapacitor electrodes due to its high conductivity [19]. The various transition metal oxides RuO_2, IrO_2, Fe_3O_4, Co_3O_4, MnO_2, NiO, etc which possessed high pseudocapacitance have been described in literature [20–24]. The bimetallic oxides $NiCo_2O_4$, $NiFe_2O_4$, $CoFe_2O_4$, $MnFe_2O_4$, $ZnFe_2O_4$ and $CuFe_2O_4$ as supercapacitor electrode material have drawn more attentions in recent years due to their high theoretical charge storage capacity, low cost, natural abundance and easy synthesis process [25,26]. Amongst these, $NiFe_2O_4$ have been mostly used in various fields including magnetic data storage devices, satellite communication, memory devices, antenna rods, transformer cores, solid oxide fuel cells, catalysis, etc due to their high electrochemical performance, good electrochemical stability, wide operating potential window, superior rate capability and easy synthesis [27–29].

The method of preparation plays a significant role in monitoring the structures and properties of the electrode materials. In literature different physical and chemical methods including pulse laser deposition [30], sol–gel [27,31], chemical combustion route [32], chemical bath deposition [27], solvothermal [33], hydrothermal [33,34], co-precipitation [35] and spray pyrolysis [36] have been used for preparation of $NiFe_2O_4$. Amongst these, spray pyrolysis which is mostly facile, effective, greatly scalable and appropriate for large area deposition, offers substantial potential for the rational design and preparation of numerous functional nanostructures with tailorable composition and surface morphology [36,37].

In this paper $NiFe_2O_4$ thin films have been prepared onto amorphous and FTO coated glass substrates by spray pyrolysis at various substrate temperatures. The effect of substrate temperature on structural, morphological, compositional, optical, electrical and electrochemical properties of $NiFe_2O_4$ thin films has been studied.

2. Experimental details

$NiFe_2O_4$ thin films have been prepared onto ultrasonically cleaned amorphous and FTO coated glass substrates using computerized chemical spray pyrolysis. The required quantities of $Ni(NO_3)_2.6H_2O$ and $Fe(NO_3)_3.9H_2O$ were dissolved separately in double-distilled water to prepare the 0.15 M precursor solutions. The Ni: Fe ratio was kept constant at 1:2 throughout the experiment. For each deposition, 5 ml $Ni(NO_3)_2.6H_2O$ and 10 ml $Fe(NO_3)_3.9H_2O$ were mixed thoroughly and 15 ml ethanol was added to make the final spraying solution 30 ml. For the preparation of $NiFe_2O_4$ thin films, the substrate temperature was varied from 400°C to 475°C at the interval of 25°C. The preparative parameters were optimized using electrochemical technique and kept constant at their optimized values namely spray rate 3–4 ml·min^{-1}; spray nozzle to substrate distance 30 cm; air as carrier gas with pressure 176520 Nm^{-2}.

Structural properties and phase identification of $NiFe_2O_4$ thin films were studied using the X-ray diffractometer (PW-3710 Philips-Model) with Cu-Kα radiation (wavelength $\lambda = 1.54056$ Å). FESEM (Model S-4800 Hitachi Corporation, Japan) was used to study the surface morphology. Stoichiometry and material compositions were studied by EDAX. To determine the optical bandgap, the optical absorption spectrum of the $NiFe_2O_4$ thin films was recorded by using UV-Vis spectrophotometer (SHIMADZU-1700). Electrical conductivity measurements were carried out using DC two-point probe method. The electrochemical measurements of $NiFe_2O_4$ thin films were carried out by using electrochemical analyzer (CHI 608D Instruments). The conventional three electrode cell configuration system was used with 1 cm^2 $NiFe_2O_4$ thin films as working electrode, platinum and saturated Ag/AgCl as a counter and reference electrodes respectively in aqueous 1M KOH electrolyte. The electrochemical measurements include the cyclic voltammetry, galvanostatic charge–discharge and electrochemical impedance spectroscopy.

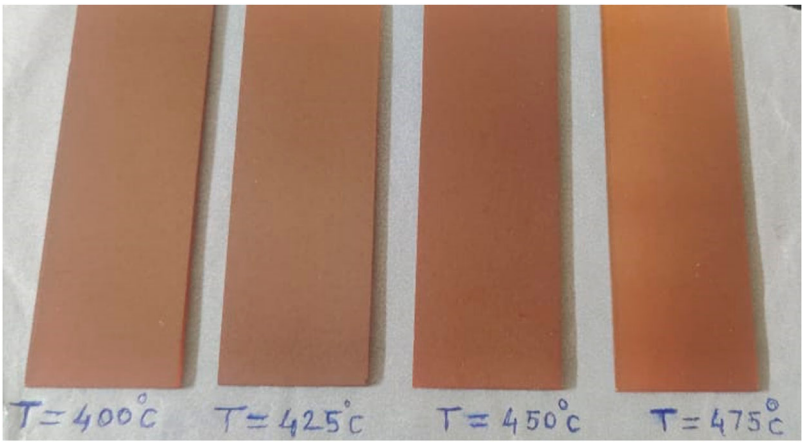

Figure 1. Photograph of $NiFe_2O_4$ thin films prepared by spray pyrolysis at various substrate temperatures.

3. Results and discussion

3.1. Growth mechanism

In spray pyrolysis, the precursor solution is pulverized through air and the fine droplets of the solution containing precursors of Ni and Fe are sprayed onto the preheated substrates. The thermal decomposition of fine droplets of $Ni(NO_3)_2.6H_2O$ and $Fe(NO_3)_3.9H_2O$ results into the formation of chocolate brown to dark brown $NiFe_2O_4$ thin films. Figure 1 shows the photograph of $NiFe_2O_4$ thin films prepared by spray pyrolysis at various substrate temperatures. The possible chemical reaction can be given as,

$$Ni(NO_3)_2 \cdot 6H_2O + 2Fe(NO_3)_3 \cdot 9H_2O \rightarrow NiFe_2O_4 + 24H_2O \uparrow + 8NO_2 \uparrow + 2O_2 \uparrow \quad (1)$$

The similar reaction mechanism for $NiFe_2O_4$ thin films prepared by spray pyrolysis has been previously reported by Karthigayan et al. [38].

3.2. Film thickness

The gravimetric weight difference method was used for measurement of thickness of $NiFe_2O_4$ thin films prepared by spray pyrolysis at various substrate temperatures. The weight of the $NiFe_2O_4$ thin films before and after deposition was measured using sensitive microbalance. The film thicknesses were found to be 455, 596, 675 and 632 nm for $NiFe_2O_4$ thin films prepared by spray pyrolysis at substrate temperatures of 400°C, 425°C, 450°C and 475°C respectively. Figure 2 shows the variation of film thickness with substrate temperature for $NiFe_2O_4$ thin films. It has been observed that as substrate temperature increases from 400°C to 450°C, film thickness increases linearly upto 675 nm and above substrate temperature of 450°C, film thickness decreases to 632 nm. The effect of substrate temperature on the film thickness can be explained as follows: the lower temperature 400°C, is not sufficient to decompose the ions of the precursor solution resulting in lower thickness. At a certain substrate temperature 450°C, decomposition occurs completely to their optimum level confirming the terminal thickness of $NiFe_2O_4$ thin films being accomplished. At higher substrate temperatures i.e. beyond the 450°C, rate of re-evaporation of solution from the surface of substrate increases and film thickness decreases. A similar type of effect of substrate temperature on the film thickness was reported earlier for NiO thin films by spray pyrolysis method [39].

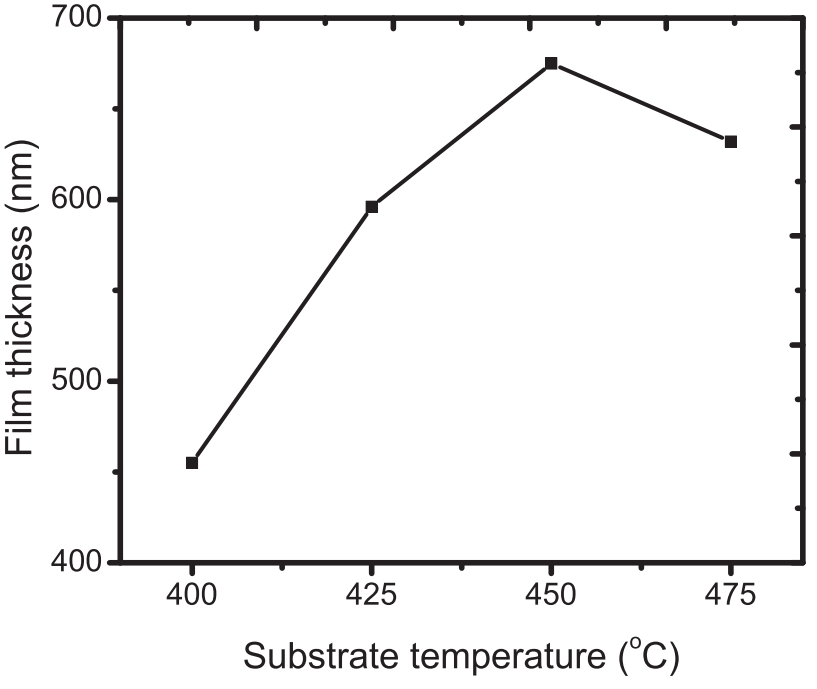

Figure 2. Variation of film thickness with substrate temperature for $NiFe_2O_4$ thin films prepared by spray pyrolysis.

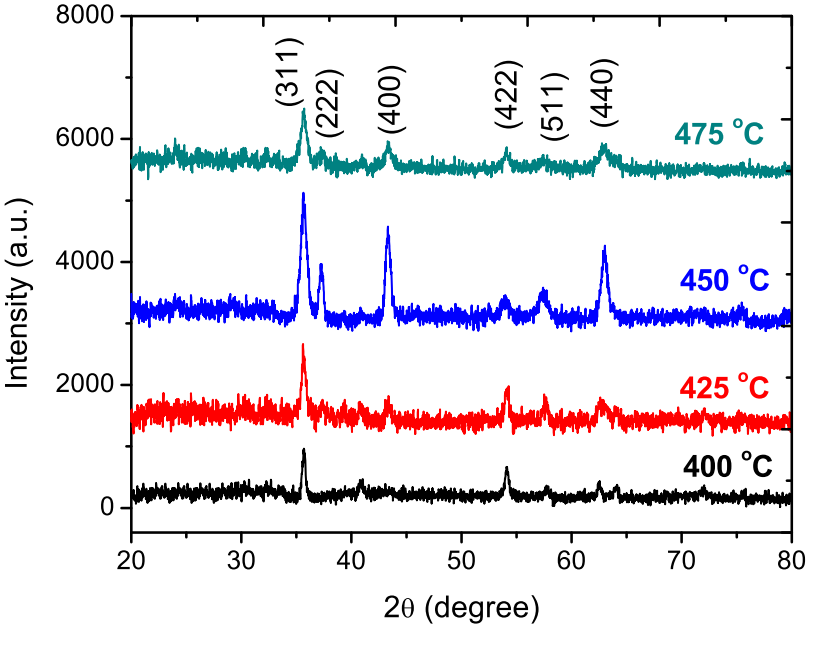

Figure 3. XRD patterns of $NiFe_2O_4$ thin films prepared by spray pyrolysis at various substrate temperatures.

3.3. X-ray diffraction

Structural analysis of $NiFe_2O_4$ thin films was carried out using X-ray diffraction with CuKα radiation within 2θ range of 20° to 80°. Figure 3 shows X-ray diffraction patterns of $NiFe_2O_4$ thin films prepared by spray pyrolysis at various substrate temperatures. Intensity peaks were observed at 2θ around

35.70°, 37.32°, 43.38°, 53.81°, 57.39° and 63.02° with corresponding planes (311), (222), (400), (422), (511) and (440) confirming the formation of cubic structure symmetry of the Fd-3 m (227) space group. The observed XRD peaks were well matched with standard JCPDS data card (86-2267) [40].

From Figure 3 it has been witnessed that the $NiFe_2O_4$ films are highly oriented along (311) plane. The peak intensity depends upon the substrate temperature used for preparation of $NiFe_2O_4$ thin films. Peak intensity increases with increasing substrate temperature attains maximum value at 450° C and decreases thereafter. At 450°C, the increased peak intensity (311) indicates improvement in the crystallinity of $NiFe_2O_4$ thin films. The decreasing crystallinity after 450°C might be due to re-evaporation of the material from the film surface or decrease in film thickness or both [41]. The comparison between standard and calculated 'd' values confirmed that $NiFe_2O_4$ have cubic crystal structure [JCPDS data card (86-2267)].

The crystallite size for (311) plane of $NiFe_2O_4$ thin films prepared by spray pyrolysis at various substrate temperatures was estimated using Debye Scherrer formula [42]. The crystallite sizes were found to be in the range of 14–21 nm. These values are less than 26 nm reported by Jamdade and coworkers [43] for chemically grown nanostructured $NiFe_2O_4$.

The lattice parameter 'a' of $NiFe_2O_4$ thin films was determined using the standard relation [44],

$$\frac{1}{d^2} = \frac{h^2 + k^2 + l^2}{a^2} \tag{2}$$

The calculated average value of lattice parameter $a = 8.3391$ Å is close to the standard JCPDS data card (86-2267), $a = 8.3379$ Å. Similar results were previously reported by Chavan et al. [37] for Al^{3+} substituted nickel ferrite thin films. The standard and calculated '*d*' values, lattice constant '*a*' and crystallite sizes for the $NiFe_2O_4$ thin films prepared by spray pyrolysis at various substrate temperatures are given in Table 1.

3.4. FESEM

Figure 4 shows the FESEM images (magnification ×200k) of $NiFe_2O_4$ thin films prepared by spray pyrolysis at various substrate temperatures (a) 400°C, (b) 425°C, (c) 450°C and (d) 475°C

Table 1. Structural data for $NiFe_2O_4$ thin films prepared by spray pyrolysis at various substrate temperatures.

Substrate temp. (°C)	2θ (°)	*d* (Å) (Cal.)	*d* (Å) (Std.)	hkl	a (Å)	*D* (nm)
400	35.63	2.518	2.513	311	8.346	14
	54.27	1.689	1.702	422		
	57.30	1.606	1.605	511		
	62.47	1.485	1.476	440		
425	35.75	2.516	2.513	311	8.338	15
	37.26	2.411	2.407	222		
	43.31	2.088	2.085	400		
	54.03	1.695	1.702	422		
	57.84	1.593	1.605	511		
	62.59	1.483	1.476	440		
450	35.51	2.527	2.513	311	8.336	21
	37.17	2.417	2.407	222		
	43.23	2.092	2.085	400		
	54.15	1.692	1.702	422		
	57.60	1.599	1.605	511		
	62.94	1.475	1.476	440		
475	35.75	2.510	2.513	311	8.335	20
	37.05	2.425	2.407	222		
	43.17	2.094	2.085	400		
	54.15	1.692	1.702	422		
	57.51	1.601	1.605	511		
	62.94	1.504	1.476	440		

2θ; Bragg's angle, d; interplanar spacing, hkl; miller indices, a; lattice constant, D; crystallite size.

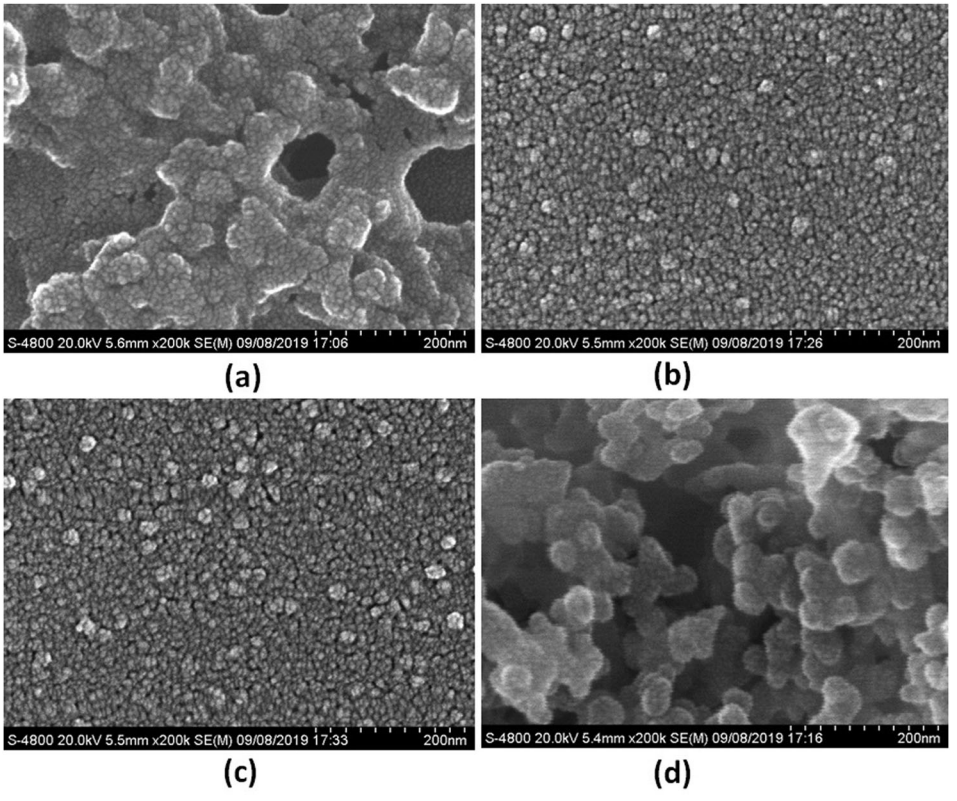

Figure 4. FESEM images (magnification × 200k) of $NiFe_2O_4$ thin films prepared by spray pyrolysis at various substrate temperatures of (a) 400°C, (b) 425°C, (c) 450°C and (d) 475°C respectively.

respectively. It shows crack free and well-distributed mesoporous spherical grain-like surface morphology. As witnessed from Figure 4 the surface morphology depends on the substrate temperature used for preparation of $NiFe_2O_4$ thin films. At substrate temperature 400°C, FESEM image shows the formation of small grain-like morphology with porous nature. FESEM results are in well agreement with the XRD results. A similar surface morphology was previously reported by Kumar and colleagues [45] for $NiFe_2O_4$ nanoparticles synthesized by one step hydrothermal method.

At substrate temperature of 425°C, FESEM shows the agglomeration of the grains with slight increase in size of spherical grains due to the interaction between the magnetic nanoparticles [37]. At substrate temperature of 450°C, films show dense and well-grown mesoporous interconnected grain-like morphology with uniform distribution of grains. Similar spherical grain-like surface morphology of $NiFe_2O_4$ was previously reported by Moradmard et al. [46]. The films prepared at 475°C shows the rougher surface as compared to films prepared at substrate temperature of 450°C. The $NiFe_2O_4$ prepared thin films prepared at substrate temperature of 450°C shows interconnected grain-like surface morphology providing maximum surface area favorable for electrochemical ion intercalation or deintercalation processes [47].

3.5. EDAX

Figure 5 shows the EDAX patterns of $NiFe_2O_4$ thin films prepared by spray pyrolysis at various substrate temperatures. The pattern shows the peaks for nickel (Ni), iron (Fe) and oxygen (O) without any impurity. Table 2 shows the compositional analysis of $NiFe_2O_4$ thin films. It proves that films are homogeneous and nearly stoichiometric. $NiFe_2O_4$ thin films prepared at substrate temperature

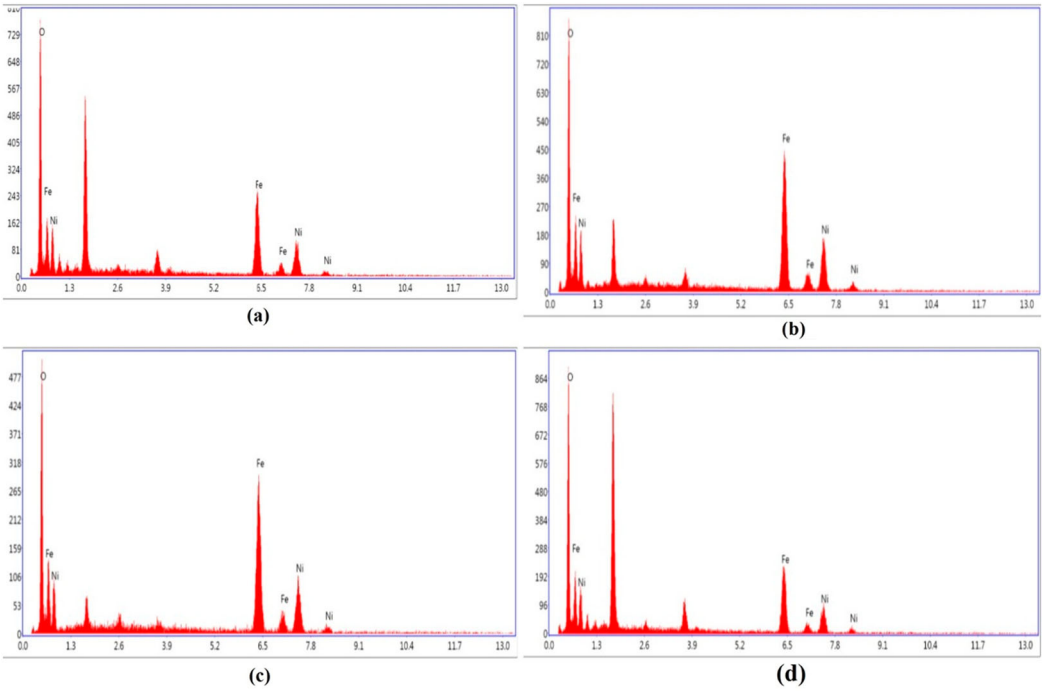

Figure 5. EDAX patterns of $NiFe_2O_4$ thin films prepared by spray pyrolysis at substrate temperatures of (a) 400°C, (b) 425°C, (c) 450°C and (d) 475°C respectively.

Table 2. Compositional analysis of $NiFe_2O_4$ thin films prepared by spray pyrolysis at various substrate temperatures.

Substrate Temp. (°C)	Atomic percentage in $NiFe_2O_4$ thin films		
	Ni	Fe	O
400	12.36	26.62	61.02
425	13.75	27.55	58.70
450	13.88	28.92	57.20
475	14.12	27.49	58.39

450°C, shows peaks of Ni, Fe and O elements with their atomic percentage 13.88%, 28.92% and 57.20% respectively confirming formation of stoichiometric $NiFe_2O_4$.

3.6. Optical

The optical absorption spectra of $NiFe_2O_4$ thin films prepared by spray pyrolysis at various substrate temperatures was recorded in the wavelength range of 400 nm to 800 nm using UV-Vis spectrophotometer. The absorption coefficient was found to be 10^4 cm^{-1}. The optical bandgap (Eg) of the $NiFe_2O_4$ thin films was estimated using the Tauc's relation [48,49]. Figure 6(a) shows the plot of $(\alpha h\upsilon)^2$ versus $h\upsilon$ for $NiFe_2O_4$ thin films prepared by spray pyrolysis at various substrate temperatures. The straight line nature of the plot specifies the direct allowed type transition [50,51].

The bandgap energies of $NiFe_2O_4$ thin films were determined from the intercepts of $(\alpha h\upsilon)^2$ of versus $h\upsilon$ plots on the energy axis (x-axis). Figure 6(b) shows the variation of bandgap energy with substrate temperature for $NiFe_2O_4$ thin films. The bandgap energies are found in the range of 2.09–2.29 eV for $NiFe_2O_4$ thin films. The bandgap energies of $NiFe_2O_4$ thin films prepared by spray pyrolysis at various substrate temperatures are mentioned in Table 3. These bandgap energies

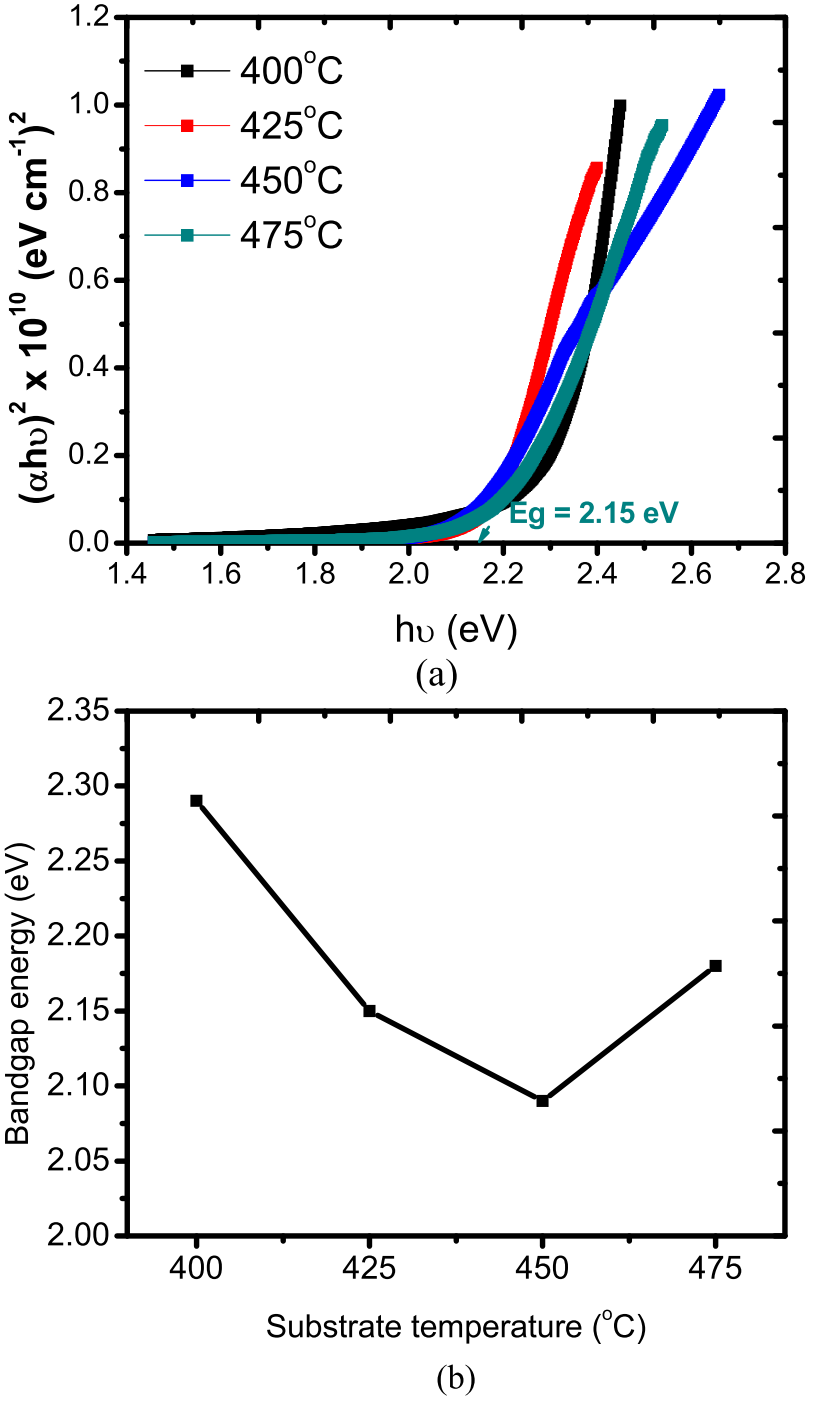

Figure 6. (a) Variation of (αhυ) ^{2} versus hυ and **(b)** Variation of bandgap energy with substrate temperature for $NiFe_2O_4$ thin films prepared by spray pyrolysis at various substrate temperatures.

are in close agreement with values of 1.78–2.72 eV reported by Tong et al. [52] and 1.87 eV reported by Zhao and colleagues [53]. The observed bandgap energies can be attributed to the spinel structure [54] and spinel ferrites have ability of exhibiting different redox states and electrochemical

Table 3. Optical and electrical properties of $NiFe_2O_4$ thin films prepared by spray pyrolysis at various substrate temperatures.

Substrate Temp. (°C)	Optical bandgap (eV)	Electrical resistivity (Ω-cm)		Activation energy (eV)	
		300 K ($\times 10^4$)	500 K ($\times 10^2$)	LT	HT
400	2.29	138	3.55	0.016	0.034
425	2.15	36.3	1.07	0.014	0.037
450	2.09	2.34	0.24	0.020	0.025
475	2.18	7.04	0.55	0.018	0.031

LT – Low temperature; HT – High temperature.

stability [55]. Generally, narrow bandgap improves the rate capability, cyclability [56] and specific capacitance [57]. Thus the observed lower bandgap of $NiFe_2O_4$ thin films is favourable for supercapacitor applications. The variation in the bandgap energy with substrate temperature can be attributed to deviation in film thickness and surface morphology of $NiFe_2O_4$ films [58].

3.7. Electrical resistivity

Electrical resistivity measurements on $NiFe_2O_4$ thin films were carried out using the DC two-point probe method in the temperature range 300 K to 500 K under dark condition. For the resistivity measurements, silver paste was applied to $NiFe_2O_4$ thin films in two-bar pattern. Figure 7 shows the variation of logρ versus inverse of absolute temperature (1000/T) for $NiFe_2O_4$ thin films prepared by spray pyrolysis at various substrate temperatures. From figure with increase in operating temperature the resistivity of $NiFe_2O_4$ thin films decreases showing typical semiconducting behavior. The electrical resistivities of $NiFe_2O_4$ thin films are given in Table 3. The lowest room temperature electrical resistivity was found to be 2.34×10^4 Ωcm for $NiFe_2O_4$ thin films prepared at 450°C, which is lower than the reported value of 3.06×10^9 Ωcm by Kambale et al. [59] for cobalt-doped

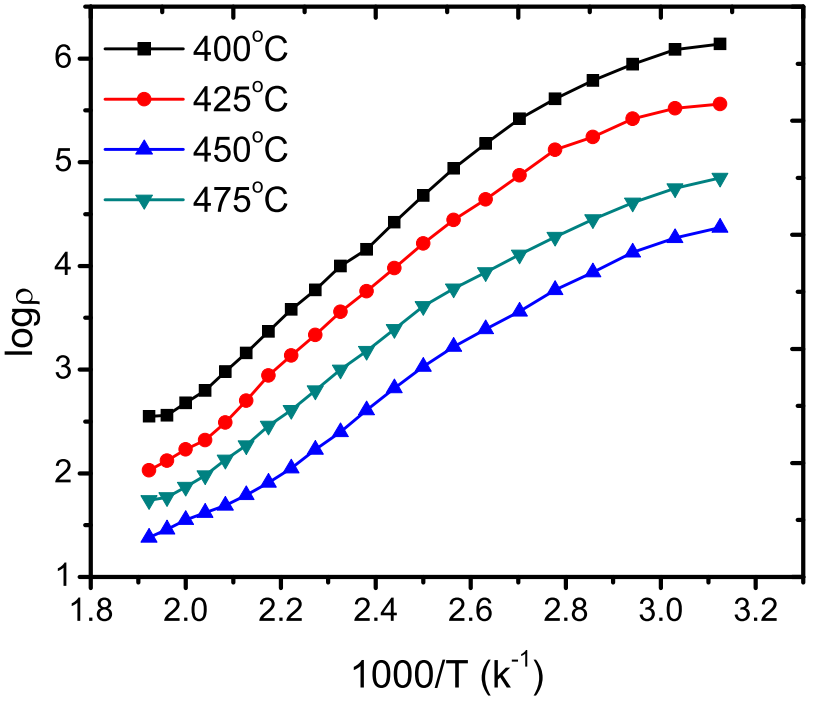

Figure 7. Variation of logρ with inverse of absolute temperature (1000/T) for $NiFe_2O_4$ thin films prepared by spray pyrolysis at various substrate temperatures.

nickel ferrites, prepared using standard ceramic technique. It has been observed that as substrate temperature increases from 400°C to 450°C electrical resistivity decreases and above 450°C resistivity increases. This behaviour is due to decrease in film thickness above substrate temperature of 450°C. Generally films with lower thicknesses show the poor crystallinity, lattice defect and higher resistivity [60].

The activation energies were determined by using Arrhenius equation [60] and are found to be in the range of 0.025–0.037 eV and 0.014–0.020 eV in high temperature and low temperature regions respectively. These values confirm that the conduction mechanism in high temperature and low temperature regions is thermally activated process considered as variable range hopping mechanism and thermionic emission respectively [61].

3.8. Electrochemical characterization

3.8.1. Cyclic voltammetry

Figure 8 shows the cyclic voltammograms (CV) at different scan rates for $NiFe_2O_4$ thin films within potential window of 0.0–0.5 V versus Ag/AgCl in aqueous 1M KOH electrolyte. The redox feature of CV curves demonstrates pseudocapacitive behaviour. CV curve reveals that intensity of the oxidation/reduction peak increases with increase in substrate temperature upto 450°C and it is associated to the redox processes observed at different sites. These redox peaks are related to the oxidation and reduction states of Ni and Fe [62]. The electrochemical reactions involved in the energy storage

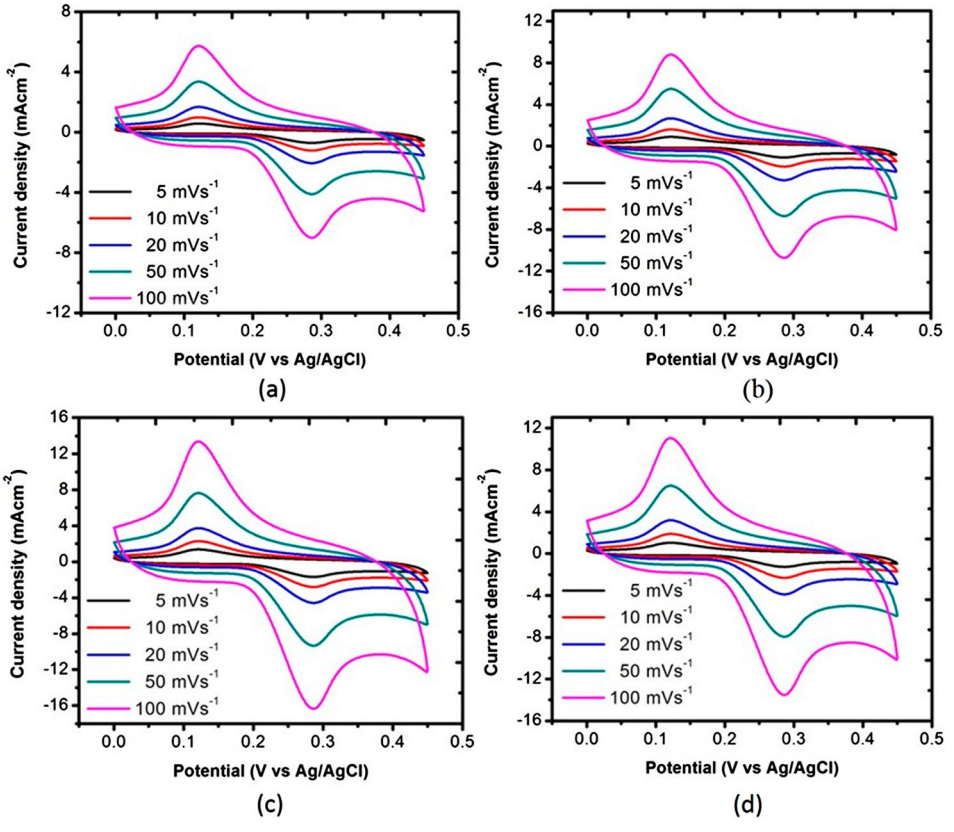

Figure 8. CV curves at different scan rates for $NiFe_2O_4$ thin films prepared by spray pyrolysis at substrate temperatures of (a) 400°C, (b) 425°C, (c) 450°C and (d) 475°C respectively.

Table 4. Specific capacitance at different scan rates from CV for $NiFe_2O_4$ thin films prepared by spray pyrolysis at various substrate temperatures.

Substrate temperature (°C) → Scan rate ($mV{\cdot}s^{-1}$)↓	400	425	450	475
		Specific capacitance from CV (Fg^{-1})		
5	383	450	591	510
10	317	395	507	450
20	270	339	423	381
50	222	277	340	310
100	188	222	300	263

mechanism (Ni^{2+}/Ni^{3+} or Fe^{3+}/Fe^{2+}) are as follows [63];

$$NiFe_2O_4 + OH^- + H_2O \leftrightarrow NiOOH + 2FeOOH + e^- \quad (3)$$

The specific capacitances (Csp) at different scan rates of $NiFe_2O_4$ thin films were calculated and are given in Table 4. It has been observed that, specific capacitance increases with increase in substrate temperature used for preparation of $NiFe_2O_4$ thin films up to 450°C and above 450°C specific capacitance decreases. This behaviour may be due to the enhancement of the surface area of $NiFe_2O_4$ thin films as seen from FESEM. Generally, the nanosized mesoporous structure of $NiFe_2O_4$ shows maximum specific capacitance than the rough surface [64] and hence above 450°C substrate temperature the specific capacitance decreases due to rough surface observed in FESEM. The maximum specific capacitance was found to be 591 Fg^{-1} at a scan rate of 5 $mV{\cdot}s^{-1}$ for $NiFe_2O_4$ thin films prepared at substrate temperature of 450°C. This value of specific capacitance is higher than 541 Fg^{-1} at scan rate 2 $mV{\cdot}s^{-1}$ for $NiFe_2O_4$ reported by Bhojane et al. [65], 287 Fg^{-1} in 1M Na_2SO_3 electrolyte reported by Jamadade and coworkers [66] for nickel doped iron hydroxide thin films and 585 Fg^{-1} at scan rate 5 $mV{\cdot}s^{-1}$ for $NiFe_2O_4$ nanocone forest on carbon textile solid state supercapacitors by Javed and colleagues [67].

Figure 9(a) shows the CV plots at scan rate of 10 $mV{\cdot}s^{-1}$ in the 1M KOH electrolyte for $NiFe_2O_4$ thin films prepared by spray pyrolysis at various substrate temperatures. The influence of scan rates on the current density of the $NiFe_2O_4$ thin films were observed from CV. As the scan rate increases redox current also increases and a small shift in peak towards positive or negative potential was observed due to kinetic irreversibility in the redox process. This kinetic irreversibility occurs due to polarization and ohmic resistance [57]. Figure 9(b) shows the variation of specific capacitance with scan rate. It shows that as scan rate increases, the area under the curve also increases but specific capacitance decreases. This is attributed to the fact that at higher scan rates the outer

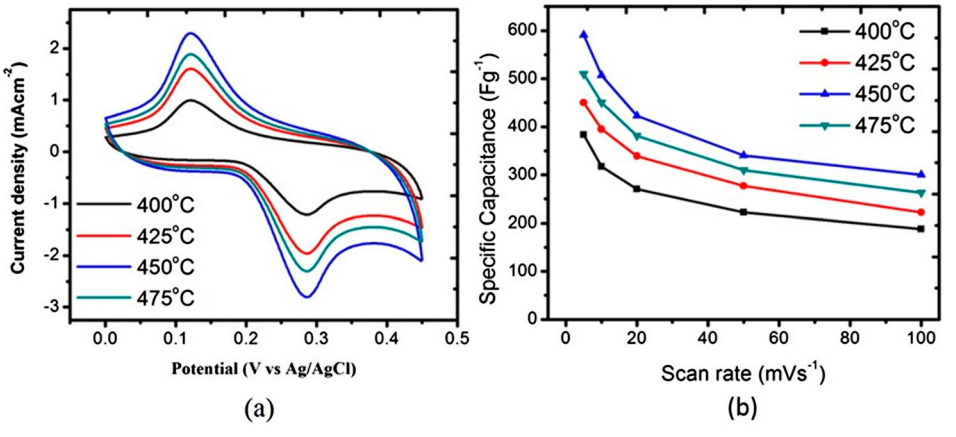

Figure 9. (a) CV plots at scan rate of 10 $mV{\cdot}s^{-1}$ and (b) plot of specific capacitance versus scan rate for $NiFe_2O_4$ thin films prepared by spray pyrolysis at various substrate temperatures.

pores of electrode material get recovered by the ions or motion of the ions on the electrodes may be fast, at the same time diffusion rate of ions in the electrolyte are slow [22, 68]. At lower scan rate, inner and outer pores of electrode material are utilized for ions propagation completely in the active electrode material [13].

3.8.2. Galvanostatic charge–discharge

To get more information about supercapacitive performance of $NiFe_2O_4$ thin films, galvanostatic charge–discharge (GCD) was performed in 1M KOH electrolyte. The charge–discharge behaviour at different current densities of $NiFe_2O_4$ thin films prepared by spray pyrolysis at various substrate temperatures is shown in Figure 10. From figure the GCD exhibits linear behaviour implying that the electrochemical redox reaction mechanism occurs at the electrolyte and active electrode materials showing the pseudocapacitive behaviour of $NiFe_2O_4$ thin films [69]. The charging curves are similar with their corresponding discharge curves with good linear voltage time profiles for all films indicates good capacitive behaviour shown in Figure 11(a). Figure 11(b) shows the plot of specific capacitance versus current density for $NiFe_2O_4$ thin films prepared by spray pyrolysis at various substrate temperatures.

The specific capacitance, specific energy and specific power were determined using relations given elsewhere [60]. The specific capacitances obtained from GCD curves at different current densities are mentioned in the Table 5. It has been observed that as substrate temperature increases the specific capacitance increases upto 450°C and decreases thereafter due to the enhancement of

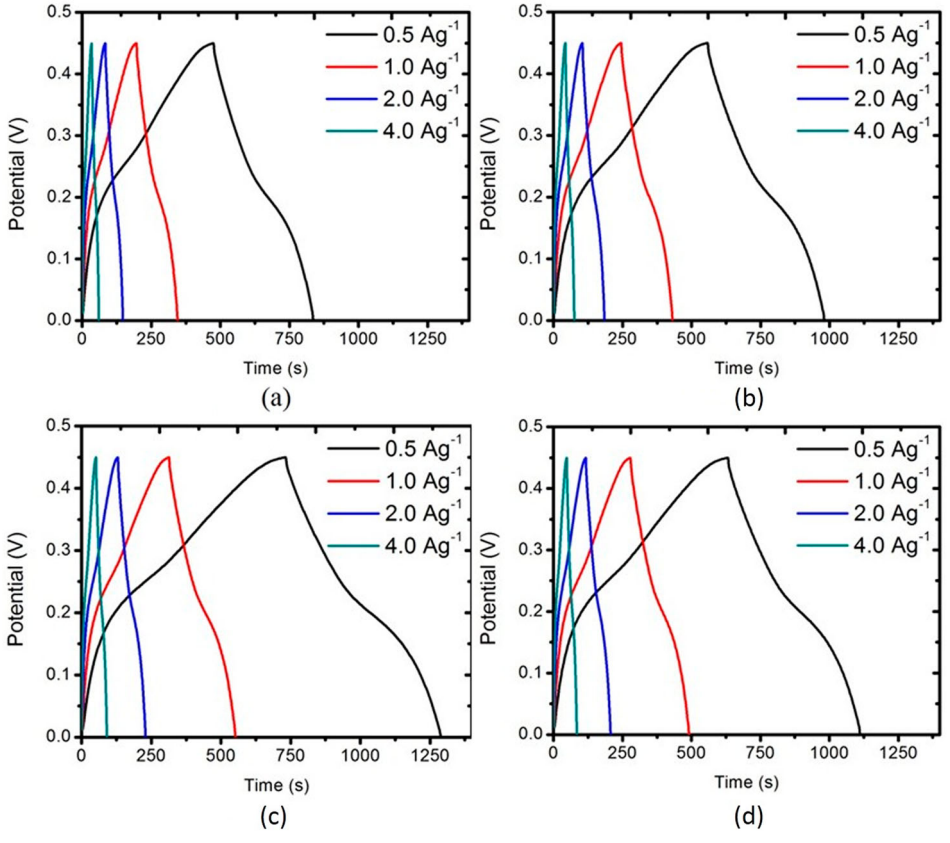

Figure 10. GCD curves at different current densities for $NiFe_2O_4$ thin films prepared by spray pyrolysis at various substrate temperatures of (a) 400°C, (b) 425°C, (c) 450°C and (d) 475°C respectively.

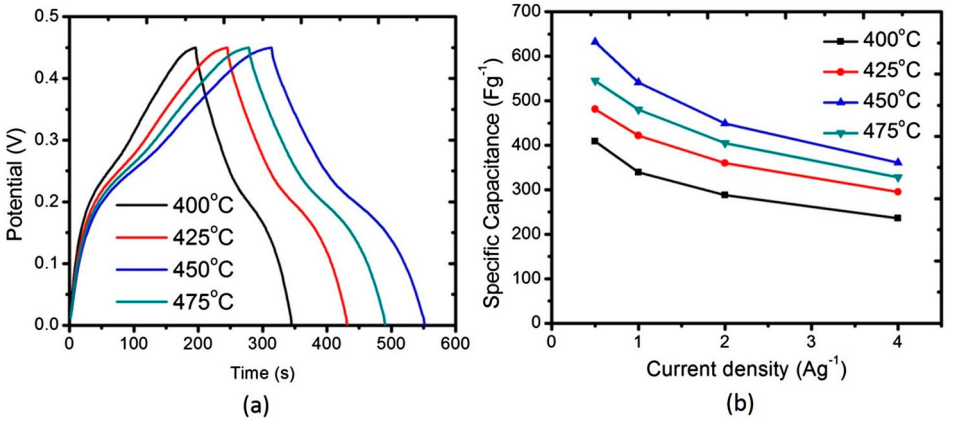

Figure 11. (a) GCD curves at current density of $1Ag^{-1}$ and (b) plot of specific capacitance versus current density for $NiFe_2O_4$ thin films prepared by spray pyrolysis at various substrate temperatures.

Table 5. Specific capacitances from GCD for $NiFe_2O_4$ thin films prepared by spray pyrolysis at various substrate temperatures.

Substrate temperature (°C) → Current density (Ag^{-1}) ↓	400	425	450	475
		Specific capacitance from GCD (Fg^{-1})		
0.5	409	481	632	545
1.0	339	422	541	480
2.0	288	360	449	405
4.0	236	295	361	328

surface morphology and film thickness. The maximum specific capacitance was found to be 632 Fg^{-1} and corresponding specific energy and specific power were found to be 17.78 $Wh{\cdot}kg^{-1}$ and 113 $kW{\cdot}kg^{-1}$ at current density of 0.5 Ag^{-1} for $NiFe_2O_4$ thin film prepared spray pyrolysis at 450°C. These values of specific capacitance are superior to 480 Fg^{-1} at current density of 1 Ag^{-1} for core–shell $NiFe_2O_4$@$NiFe_2O_4$ nanofibers reported by Wang and co-workers [3].

3.8.3. Electrochemical impedance spectroscopy

To understand the benefit of the material for electrochemical supercapacitors, impedance spectra of $NiFe_2O_4$ thin films were recorded in the frequency range from 1 Hz to 100 kHz. Figure 12 shows the Nyquist plot for $NiFe_2O_4$ thin films prepared by spray pyrolysis at various substrate temperatures. The diameter of semicircle indicates the charge transfer resistance (Rct) at the electrode electrolyte interface. From figure, it has been observed that as the substrate temperature increases upto 450°C, the diameter of semicircle decreases and increases thereafter which indicates that charge transfer resistance of $NiFe_2O_4$ depends on the substrate temperature. The $NiFe_2O_4$ thin film prepared at 450°C has the lowest Rct indicating easy charge transfer process. From Table 6, the $NiFe_2O_4$ thin film prepared at 400°C showed highest value of Rct due to incomplete decomposition whereas for 475°C showed higher Rs and Rct due to lower film thickness.

4. Conclusions

In conclusion, the $NiFe_2O_4$ thin films have been successfully prepared using chemical spray pyrolysis at various substrate temperatures. The films are of polycrystalline nature and well adherent on the substrates. XRD patterns showed the formation of cubic crystal structure with Fd-3 m (227) space group. Crystallite size is found in the range of 14–21 nm. FESEM images showed crack free, well defined, uniform, mesoporous spherical grain-like surface morphology. EDAX study

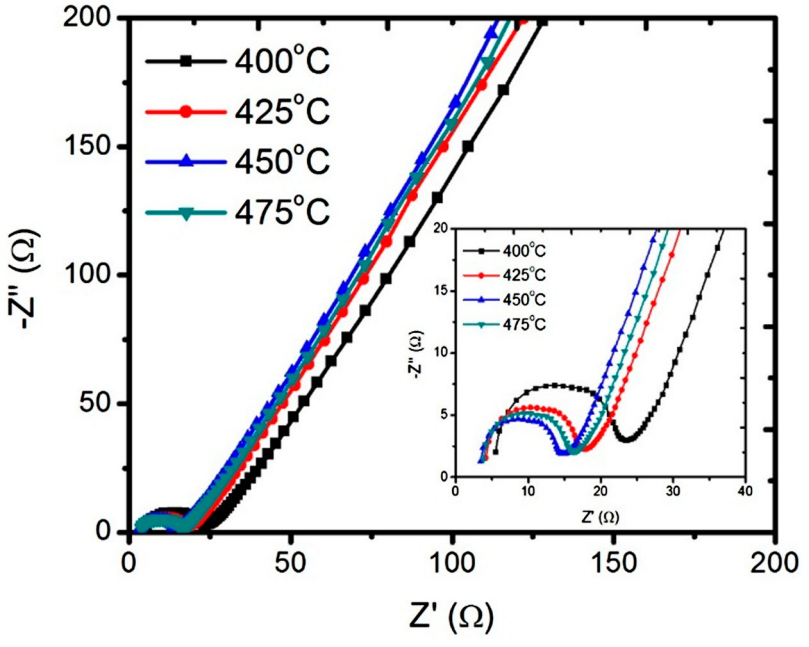

Figure 12. Nyquist plot for $NiFe_2O_4$ thin films prepared by spray pyrolysis at various substrate temperatures (The inset shows the enlarged view of Nyquist plots).

Table 6. Nyquist data for $NiFe_2O_4$ thin films prepared by spray pyrolysis at various substrate temperatures.

Substrate temperature (°C)	Rs (Ω)	Rct (Ωcm^2)
400	4.75	25
425	3.25	19.10
450	2.75	16.05
475	2.85	17.55

confirmed nearly stoichiometric deposition of $NiFe_2O_4$ thin films. The absorption coefficient was found to be in the range of 10^4 cm^{-1} with direct allowed type transition having bandgap energies in the range of 2.09–2.29 eV. The $NiFe_2O_4$ thin film based supercapacitor exhibited superior electrochemical performance with specific capacitance of 591 Fg^{-1} at a scan rate of 5 $mV{\cdot}s^{-1}$ from CV and 632 Fg^{-1} at a current density of 0.5 Ag^{-1} from GCD 1M KOH electrolyte. The remarkable mesoporous structure and electrical resistivity allows $NiFe_2O_4$ electrodes to be auspicious materials for next generation high performance supercapacitors.

Disclosure statement

No potential conflict of interest was reported by the author(s).

ORCID

Abhijit A. Yadav http://orcid.org/0000-0002-3486-4099

References

[1] Yadav BK, Singh P, Yadav CP, et al. Synthesis and characterization of $ZnSe_{1-x}Te_x$ thin films. Phase Transitions. 2021;94(5):326–337.

[2] Patil NM, Nilange SG, Jundale VA, et al. Structural, optical and electrical properties of spray-deposited Fe-doped nanocrystalline $ZnS_{0.2}Se_{0.8}$ thin films. Phase Transitions. 2021;94:6–8. 493-510.
[3] Wang Q, Gao H, Qin X, et al. Fabrication of $NiFe_2O_4$@$CoFe_2O_4$ core-shell nanofibers for high performance supercapacitors. Mater Res Exp. 2020;7:015020.
[4] Jeyabanu K, Devendran P, Manikandan A, et al. Preparation and characterization studies of La doped CuS nanospheres by microwave irradiation for high performance supercapacitors. Phys B: Cond Matter. 2019;573:92–101.
[5] Khalid S, Cao C, Wang L, et al. A high performance solid state asymmetric supercapacitor device based upon $NiCo_2O_4$ nanosheets // MnO_2 microspheres. RSC Adv. 2016;6:70292–70302.
[6] Khalid S, Cao C, Ahmad A, et al. Microwave assisted synthesis of mesoporous $NiCo_2O_4$ nanosheets as electrode material for advanced flexible supercapacitors. RSC Adv. 2015;5:33146–33154.
[7] Zhu Y, Cao C, Tao S, et al. Ultrathin nickel hydroxide and oxide nanosheets: synthesis, characterizations and excellent supercapacitor performances. Sci Rep. 2015;4:5787.
[8] Khalid S, Cao C, Wang L, et al. Microwave assisted synthesis of porous $NiCo_2O_4$ microspheres: application as high performance asymmetric and symmetric supercapacitors with large areal capacitance. Sci Rep. 2016;6:22699.
[9] Wu Y, Cao C. The way to improve the energy density of supercapacitors: progress and perspective. Sci China Mater. 2018;61:1517–1526.
[10] Xu X, Cao C, Zhu Y. Facile synthesis of single crystalline mesoporous hematite nanorods with enhanced supercapacitive performance. Electrochim Acta. 2015;155:257–262.
[11] Jundale VA, Yadav AA. Precursor solution concentration-dependent electrochemical properties of $CoFe_2O_4$ thin films. J Mater Sci Mater Electron. 2022;33:19612–19626.
[12] Yadav AA, Chavan UJ. Electrochemical supercapacitive performance of spray deposited $NiSnO_3$ thin films. Thin Solid Films. 2017;634:33–39.
[13] Su DY, Liu ZG, Jiang L, et al. Conducting polymers in supercapacitor application. IOP Conf Series: Earth and Environ Sci. 2019;267:042048.
[14] Kennaz H, Harat A, Guellati O, et al. Synthesis and electrochemical investigation of spinel cobalt ferrite magnetic nanoparticles for supercapacitor application. J Solid State Electrochem. 2018;22:835–847.
[15] Bashir B, Rahman A, Muhammad HS, et al. Copper substituted nickel ferrite nanoparticles anchored onto the graphene sheets as electrode materials for supercapacitors fabrication. Ceram Inter. 2019;45:6759–6766.
[16] Yari A, Fathabad SH. A high-performance supercapacitor based on cerium molybdate nanoparticles anchored on N, P co-doped reduced graphene oxide nanocomposite as the electrode. J Mater Sci: Mater Electron. 2020;31:1–12.
[17] Sagu JS, Wijayantha KGU, Tahir AA. The pseudocapacitive nature of $CoFe_2O_4$ thin films. Electrochim Acta. 2017;246:870–878.
[18] Yu M, Feng X. Thin-Film electrode-based supercapacitors. Joule. 2019;3:338–360.
[19] Conway BE. Transition from "supercapacitor" to "battery" behavior in electrochemical energy storage. J Electrochem Soc. 1991;138:1539–1548.
[20] Idrissi L, Tahiri N, El Bounagui O, et al. Theoretical investigation of physical properties of the spinel $ZnFe_2O_4$ compound: Ab-initio calculation. Ph Transit. 2021;94(3-4):134–146.
[21] Maazouzi AEL, Masrour R, Jabar A. Thickness-dependent magnetic properties of inverse spinel Fe_3O_4. Ph Transit. 2020;93(7):733–740.
[22] Yadav AA, Deshmukh TB, Deshmukh RV, et al. Electrochemical supercapacitive performance of hematite α-Fe_2O_3 thin films prepared by spray pyrolysis from non-aqueous medium. Thin Solid Films. 2016;616:351–358.
[23] Kore RM, Lokhande BJ. A robust solvent deficient route synthesis of mesoporous Fe_2O_3 nanoparticles as supercapacitor electrode material with improved capacitive performance. J Alloy Compd. 2017;725:129–138.
[24] Naeem F, Naeem S, Zhao Y, et al. Tio_2 nanomembranes fabricated by atomic layer deposition for supercapacitor electrode with enhanced capacitance. Nano Res Lett. 2019;14:92.
[25] Nikam SM, Sharma A, Rahaman M, et al. Pulsed laser deposited $CoFe_2O_4$ thin films as supercapacitor electrodes. RSC Adv. 2020;10:19353–19359.
[26] Vadiyar MM, Bhise SC, Patil SK, et al. Mechanochemical growth of porous $ZnFe_2O_4$ nano-flakes thin film as electrode for supercapacitor application. RSC Adv. 2013;5:1–3.
[27] Bandgar S, Vadiyar MM, Ling Y-C, et al. Metal precursor dependent synthesis of $NiFe_2O_4$ thin films for high performance flexible symmetric supercapacitor. ACS Appl Ener Mater. 2018;1(2):638–648.
[28] Gunjakar JL, More AM, Gurav KV, et al. Chemical synthesis of spinel nickel ferrite ($NiFe_2O_4$) nano-sheets. Appl Surf Sci. 2008;254:5844–5848.
[29] Saravanakumar B, Rani BJ, Ravi G, et al. Reducing agent ($NaBH_4$) dependent structure, morphology and magnetic properties of nickel ferrite ($NiFe_2O_4$) nanorods. J Magn Mag Mater. 2017;428:78–85.
[30] Dixit G, Singh JP, Srivastava RC, et al. Structural and magnetic behavior of $NiFe_2O_4$ thin film grown by pulsed laser deposition. Ind J Pure Appl Phy. 2010;48(4):287–291.

[31] Montemayor SM, Garcia-Cerda LA, Torres-Lubian JR, et al. Comparative study of the synthesis of $CoFe_2O_4$ and $NiFe_2O_4$ in silica through the polymerized complex route of the sol-gel method. J Sol-Gel Sci Tech. 2007;42:181–186.
[32] De M, Bera G, Tewari HS. Characterization of magnesium substituted nickel ferrites nano-particles synthesized using combustion technique. Int J Math Phys Sci Res. 2015;3:71–76.
[33] Aparna ML, Grace AN, Sathyanarayanan P, et al. A comparative study on the supercapacitive behavior of solvothermally prepared metal ferrite (MFe_2O_4, M = Fe, Co, Ni, Mn, Cu, Zn) nanoassemblies. J Alloys Compd. 2018;745:385–395.
[34] Naidu KC, Madhuri W. Hydrothermal synthesis of $NiFe_2O_4$ nano-particles: structural, morphological, optical, electrical and magnetic properties. Bull Mater Sci. 2017;40(2):417–425.
[35] Albuquerque AS, Ardisson JD, Macedo WAA, et al. Structure and magnetic properties of nanostructured Ni-ferrite. J Magn Mag Mater. 2001;226-230:1379–1381.
[36] Leng J, Wang Z, Wang J, et al. Advances in nanostructures fabricated *via* spray pyrolysis and their applications in energy storage and conversion. Chem Soc Rev. 2019;48:3015–3072.
[37] Chavan AR, Birajdar SD, Chilwar RR, et al. Structural, morphological, optical, magnetic and electrical properties of Al^{3+} substituted nickel ferrite thin films. J Alloys Compd. 2018;735:2287–2297.
[38] Karthigayan N, Manimuthu P, Priya M, et al. Synthesis and characterization of $NiFe_2O_4$, $CoFe_2O_4$ and $CuFe_2O_4$ thin films for anode material in Li-ion batteries, nanomater. Nanotech. 2017;7:1–5.
[39] Yadav AA, Chavan UJ. Influence of substrate temperature on electrochemical supercapacitive performance of spray deposited nickel oxide thin films. J Electroanal Chem. 2016;782:36–42.
[40] JCPDS data card (86-2267).
[41] Yadav AA, Chavan UJ. Electrochemical supercapacitive performance of spray deposited Co_3O_4 thin film nanostructures. Electrochim Acta. 2017;232:370–376.
[42] Henry J, Daniel T, Balasubramanian V, et al. Synthesis and characterisation of Cu_2Se thin films doped with divalent cation (Cd^{2+}) by the chemical bath deposition method. Phase Transitions. 2021;94:567–576.
[43] Jamadade VS, Pusawale SN, Pathan HM, et al. Characterization of chemically grown nanostructured $NiFe_2O_4$. AIP Conf Proceed. 2012;1451:88–90.
[44] Agouriane E, Essoumhi A, Razouk A, et al. X-ray diffraction and mossbauer studies of $NiFe_2O_4$ nanoparticles obtained by co-precipitation method. J Mater Environ Sci. 2016;7(12):4614–4619.
[45] Kumar N, Kumar A, Chandrasekaran S, et al. Synthesis of mesoporous $NiFe_2O_4$ nanoparticles for enhanced supercapacitive performance. J Clean Ener Techn. 2018;6:51–55.
[46] Moradmard H, Shayesteh SF. The variation of magnetic properties of nickel ferrite by annealing. Manuf Sci Techn. 2015;3:141–145.
[47] Ingole RS, Lokhande BJ. Effect of pyrolysis temperature on structural, morphological and electrochemical properties of vanadium oxide thin films. J Anal Appl Pyrol. 2016;120:434–440.
[48] Shetty C, Shastrimath VVD, Bairy R. Tuning the structural, morphological and optical properties of Sr-doped BFO thin films. Ph Transit. 2022;95(3):202–211.
[49] Ganesh Kumar K, Balaji Bhargav P, Gnana Prakash D, et al. Investigations on SILAR coated CZTS thin films for solar cells applications. Phase Transitions. 2021;94(6-8):556–566.
[50] Joshi GP, Saxena NS, Mangal R, et al. Band gap determination of Ni-Zn ferrites. Bull Mater Sci. 2003;26 (4):387–389.
[51] Yadav AA. Spray deposition of tin oxide thin films for supercapacitor applications: effect of solution molarity. J Mater Sci Mater Electron. 2016;27:6985–6991.
[52] Tong S-K, Chi P-W, Kung S-H, et al. Tuning bandgap and surface wettability of $NiFe_2O_4$ driven phase transition. Sci Reports. 2018;8:1338.
[53] Zhao DF, Yang H, Li RS, et al. Fabrication of nickel ferrite- graphene nanocomposites and their photocatalytic properties. Mater Res Inno. 2014;18:519–523.
[54] Ravindra AV, Chandrika M, Rajesh C, et al. Simple synthesis structural and optical properties of cobalt ferrite nanoparticles. European Phy J Plus. 2019;134:296.
[55] Bhujun B, Tan MTT, Shanmugam AS. Study of mixed ternary transition metal ferrites as potential electrodes for supercapacitor applications. Results Phys. 2017;7:345–353.
[56] Jhan Y-R, Duh J-G. Electrochemical performance and low discharge cut-off voltage behavior of ruthenium doped $Li_4Ti_5O_{12}$ with improved energy density. Electrochim Acta. 2012;63:9–15.
[57] Sharif S, Yazdani A, Rahimi K. Incremental substitution of Ni with Mn in $NiFe_2O_4$ to largely enhance its supercapacitance properties. Sci Rep. 2020;10:10916.
[58] Venkatachalam V, Jayavel R. Novel synthesis of Ni-ferrite ($NiFe_2O_4$) electrode material for supercapacitor applications. AIP Conf Proceed. 2015;1667:140016.
[59] Kambale RC, Shaikh PA, Kamble SS, et al. Effect of cobalt substitution on structural, magnetic and electric properties of nickel ferrite. J Alloys Compd. 2009;478:599–603.
[60] Yadav AA. Physical and electrochemical properties of spray-deposited Co_3O_4thin films. Ph Transit. 2021;94 (10):691–704.

[61] Nilange SG, Patil NM, Yadav AA. Growth and characterization of spray deposited quaternary Cu_2FeSnS_4 semiconductor thin films. Phys B. 2019;560:103–110.
[62] Gibin SR, Sivagurunathan P. Synthesis and characterization of nickel cobalt ferrite ($Ni_{1-x}Co_xFe_2O_4$) nano particles by co-precipitation method with citrate as chelating agent. J Mater Sci Mater Electron. 2017;28:1985–1996.
[63] Gao X, Wang W, Bi J, et al. Morphology-controllable preparation of $NiFe_2O_4$ as high performance electrode material for supercapacitor. Electrochim Acta. 2019;296:181–189.
[64] Senthikumar B, Selvan RK, Vinothbabu P, et al. Structural, magnetic, electrical and electrochemical properties of $NiFe_2O_4$ synthesized by the molten salt technique. Mater Chem Phy. 2011;130:285–292.
[65] Bhojane P, Sharma A, Pusty M, et al. Synthesis of ammonia-assisted porous nickel ferrite ($NiFe_2O_4$) nanostructures as an electrode material for supercapacitors. J Nanosci Nanotech. 2017;17:1387–1392.
[66] Jamadade VS, Fulari VJ, Lokhande CD. Supercapacitive behavior of electrosynthesized marygold-like structured nickel doped iron hydroxide thin film. J Alloys Compd. 2011;509:6257–6261.
[67] Javed MS, Zhang C, Chen L, et al. Hierarchical mesoporous $NiFe_2O_4$ nanocone forest directly growing on carbon textile for high performance flexible supercapacitors. J Mater Chem A. 2016;4:8851–8859.
[68] Yan J, Khoo U, Sumboja A, et al. Facile coating of manganese oxide nanowires with high-performance capacitive behavior. ACS Nano. 2010;4:4247–4255.
[69] Ismail FM, Ramadan M, Abdellah AM, et al. Mesoporous spinel manganese zinc ferrite for high-performance supercapacitors. J Electroanal Chem. 2018;817:111–117.